



Article

# Innovative Process Strategies in Powder-Based Multi-Material Additive Manufacturing

Robert Setter <sup>1,2,\*</sup> , Jan Hafenecker <sup>2,3</sup>, Richard Rothfelder <sup>2,4,5</sup>, Sebastian-Paul Kopp <sup>2,5,6</sup>, Stephan Roth <sup>2,5,6</sup>, Michael Schmidt <sup>2,4,5,6</sup> , Marion Merklein <sup>2,3</sup> and Katrin Wudy <sup>1,2</sup>

- <sup>1</sup> Professorship of Laser-Based Additive Manufacturing, Department of Mechanical Engineering, TUM School of Engineering & Design, Technical University of Munich, Boltzmannstr. 15, 85748 Garching, Germany
  - <sup>2</sup> Collaborative Research Center 814 (CRC 814), Friedrich-Alexander University Erlangen-Nuremberg, Am Weichselgarten 10, 91058 Erlangen, Germany
  - <sup>3</sup> Institute of Manufacturing Technology, Department Mechanical Engineering, Friedrich-Alexander University Erlangen-Nuremberg, Egerlandstraße 13, 91058 Erlangen, Germany; jan.hafenecker@fau.de (J.H.)
  - <sup>4</sup> Institute of Photonic Technologies, Department Mechanical Engineering, Friedrich-Alexander University Erlangen-Nuremberg, Konrad-Zuse-Straße 3/5, 91052 Erlangen, Germany; richard.rothfelder@pt.uni-erlangen.de (R.R.)
  - <sup>5</sup> Erlangen Graduate School in Advanced Optical Technologies (SAOT), Friedrich-Alexander University Erlangen-Nuremberg, 91052 Erlangen, Germany
  - <sup>6</sup> Bayerisches Laserzentrum GmbH, 91052 Erlangen, Germany; s-p.kopp@blz.org (S.-P.K.)
- \* Correspondence: robert.setter@tum.de

**Abstract:** Multi-material additive manufacturing (AM) attempts to utilize the full benefits of complex part production with a comprehensive and complementary material spectrum. In this context, this research article presents new processing strategies in the field of polymer- and metal-based multi-material AM. The investigation highlights the current progress in powder-based multi-material AM based on three successfully utilized technological approaches: additive and formative manufacturing of hybrid metal parts with locally adapted and tailored properties, material-efficient AM of multi-material polymer parts through electrophotography, and the implementation of UV-curable thermosets within the laser-based powder bed fusion of plastics. Owing to the complex requirements for the mechanical testing of multi-material parts with an emphasis on the transition area, this research targets an experimental shear testing set-up as a universal method for both metal- and polymer-based processes. The method was selected based on the common need of all technologies for the sufficient characterization of the bonding behavior between the individual materials.

**Keywords:** additive manufacturing; multi-material additive manufacturing; polymers; metals; shear testing; mechanical testing; powder bed fusion; binder jetting; electrophotography; vibration dispenser



**Citation:** Setter, R.; Hafenecker, J.; Rothfelder, R.; Kopp, S.-P.; Roth, S.; Schmidt, M.; Merklein, M.; Wudy, K. Innovative Process Strategies in Powder-Based Multi-Material Additive Manufacturing. *J. Manuf. Mater. Process.* **2023**, *7*, 133. <https://doi.org/10.3390/jmmp7040133>

Academic Editor: Steven Y. Liang

Received: 24 May 2023  
Revised: 2 June 2023  
Accepted: 13 July 2023  
Published: 24 July 2023



**Copyright:** © 2023 by the authors. Licensee MDPI, Basel, Switzerland. This article is an open access article distributed under the terms and conditions of the Creative Commons Attribution (CC BY) license (<https://creativecommons.org/licenses/by/4.0/>).

## 1. Introduction

State-of-the-art multi-material processing, like multi-material injection molding, is often limited by extensive tooling effort and limited complexity in part design. Additive manufacturing (AM) represents a promising technology to overcome these limitations. A broad selection of energy input strategies and process enhancements, as well as the possibility to selectively deposit different materials, enables the expansion of the state-of-the-art material spectrum, as well as the utilization of currently untapped material combinations. Based on the process strategy, multi-material AM can be divided into two sectors: multi-material AM and hybrid multi-material AM [1,2]. The latter sequentially combines conventional processing techniques with AM to create multi-material parts. This investigation demonstrates the scientific progress in powder-based multi-material AM based on three successfully utilized experimental technologies in the field of polymer- and metal-based processing. The framework of this article and the research target of this investigation is divided into three aspects:

1. Introduction of three successfully utilized experimental multi-material AM technologies: one from the field of hybrid metal-based multi-material AM and two from the field of polymer-based multi-material AM;
2. Identification of research-based overlaps and comparable targets of the introduced processes;
3. Presentation of experimental shear testing results to characterize the transition area between different materials, which is identified as a common challenge for all three processes.

As described above, the first target of this research is the introduction of three successfully utilized technological approaches to create multi-material polymer and metal parts.

Technology 1 is represented by hybrid AM and vibrational microfeeding in the laser-based powder bed fusion of metals (PBF-LB/M) to locally adapt and tailor part properties. The used vibration dispenser enables the possibility to add alloying elements layer-wise to selectively adjust the alloy composition only where it is wanted and/or needed, and to further limit the contamination of the remaining powder.

Technology 2 is the material-efficient AM of multi-material polymer parts through electrophotography. This technology makes it possible to electrically charge and selectively place different polymer powders within the powder bed of the laser-based powder bed fusion of plastics (PBF-LB/P). This increases process flexibility, which is adjustable for each single layer. The process becomes almost independent of powder flowability, and the powder efficiency is significantly increased due to selective and precise powder application.

Technology 3 is the selective deposition of UV-curable thermosets within the powder bed of PBF-LB/P. This approach represents one of the first AM technologies to successfully combine thermosets and polymers within a single AM process. The utilization of drop-on-demand print head technology enables the deposition of liquids with near-unlimited complexity.

Based on the lessons learned from the process development of all three technologies, research-based overlaps and comparable research targets are identified. An experimental set-up for mechanical shear testing is selected to characterize the transition area between the constituents of multi-material polymer and metal parts. As the transferability of results represents a common challenge for the mechanical testing of multi-material AM parts due to part and material complexity, the decision was made to use a unified method for polymers and metals with a simplified sample geometry. Before individually describing the three technologies of interest in detail, the respective state of research and technology of AM of multi-material polymer and metal parts is highlighted.

## 2. State of Research

### 2.1. Laser-Based Additive Manufacturing of Multi-Material Metal Parts

The state of research in the laser-based AM of multi-material metal parts is dependent on the specific process. The laser-based directed energy deposition of metals (DED-LB/M) and its basic principle allow the combination of different materials with less technological effort in comparison with the laser-based powder bed fusion of metals (PBF-LB/M) [3]. The reason for this difference is the way in which the powder feedstock is transported from the powder reservoir to the process zone. For a DED machine, a powder feeder is used, from which powder is transported via a gas stream through a tube system to the powder nozzle. The powder feed rate can be controlled and changed over time. By adding another powder feeder to the same tube system, different materials can be transported and processed with the same nozzle without the need for a critical adjustment to the setup. The focus of this work is PBF-LB/M; therefore, the progress in DED multi-material fabrication will not be discussed in detail. For a comprehensive overview of the state of the art in this field, the work of Feenstra et al. [4] is recommended. For PBF-LB/M, the requirements for multi-material parts are significantly more complex. Most commercially available powder bed systems have only a single powder container, from which powder is transported to the whole build area of the machine via a coating mechanism. Even by

adding a second powder-storage container, there is the possibility to add a completely new layer of powder. This would allow the option to create multi-material parts with a change in alloy composition in the z-direction, but the feedstocks would be irreversibly mixed. PBF-LB/M powder can be reused many times under standard boundary conditions, but mixed powder feedstock could not even be used to create the same part again. Premixing powders can be used to create parts from alloys that are hard to produce otherwise by in situ alloy formation, for example, to produce parts from high-entropy alloys [5]. The resulting parts then consist of a homogeneous alloy and cannot be considered a multi-material part. Therefore, the system technology must be adapted in another fashion to create true multi-material parts. Anstaett et al. demonstrated an approach for 2D multi-material parts [6] creating specimens consisting of steel and a copper alloy. In a more recent study, Wang et al. presented their work on multi-material parts in the z-direction, again a mixture of steel and copper alloy [7]. Walker et al. demonstrated a new system for 3D multi-material parts, modifying the coating mechanism and removing powder with a vacuum cleaner to prevent feedstock contamination [8].

### *2.2. Introduction Technology 1: Hybrid AM and Vibrational Microfeeding in PBF-LB/M to Locally Adapt and Tailor Properties*

The general goal of the combination of AM and forming operations is to gain the benefits of both worlds. The advantages of AM are the possibility to manufacture metal parts with intricate geometry and integrated function elements, e.g., cooling channels [9]. Forming allows the generation of parts with high volume and good surface quality in short manufacturing cycles, especially when compared with AM in general. The sheet metal used as a substrate for additively manufactured parts can be used as the base material of AM-formed parts [10]. By creating complex geometry on the substrate's surface, the design freedom of AM is combined with the processing speed of forming operations. The materials identified to create these parts are mainly Ti6Al4V and 316L, whereas a combination of similar materials can be used as well. Ti6Al4V was chosen because of its value for medical and aerospace applications. But Ti-based alloy is challenging for forming due to its martensitic microstructure in its as-built condition [11]. Formability can be increased by an adapted scanning strategy during the PBF-LB/M process [12] and/or by adding additional alloying elements for beta-stabilization [13]. As described in Section 2.1, the local application for powder in a commercial system is limited to premixing the feedstock. This would alter the part's properties over the complete volume, also destroying the beneficial properties of Ti6Al4V at the surface. Material flow during forming is only necessary in a small area. Global in situ alloying is, therefore, not an answer to the request. Another option for locally changing material composition and creating graded part properties, besides the already described approaches, is vibrational microfeeding. This is a viable option for metals and polymers, presented in [14]. It evolves a hard cut between material A and material B, and enables the creation of graded part properties by adding only small amounts of powder to specific part areas, which are completely molten during the process. This allows for locally adapted part properties without the need for a dedicated powder-removal system. A small robotic arm is placed in the build chamber of a PBF-LB/M system, which moves a piezo actor linked to a small glass tube filled with additional alloying elements with decreasing diameter to the end facing the powder bed. When moved into position, the applied voltage generates vibration in the piezo actor, releasing small amounts of powder from the glass tube and onto the powder bed's surface. The mass of the powder is small enough to be molten completely during the scanning of the respective layer. Owing to the developing gas plume over the melt pool, single powder grains may leave the process area, but the amount of powder feedstock contamination should not be higher than the limit for vacuum cleaning the entire layer. Furthermore, experiments have shown that the use of beam shaping can reduce spatter formation significantly [15], reducing contamination even further. Owing to the additional height of the powder deposition in addition to the normal layer thickness, adapted scanning

strategies for higher layer thickness are required to compensate for the increase in and avoid the deformation of the resulting part. With the vibrational microfeeding of the material properties, in this case, increased formability can be realized only where needed. This could also be used in other material combinations to locally increase the hardness of steel parts on the surface, for example.

### 2.3. Laser-Based Additive Manufacturing of Thermoplastic Multi-Material Polymer Parts

Generating multi-material polymer parts using laser-based AM generally requires the realization of a defined, heterogeneous thermoplastic powder layer consisting of different materials. If the thermal processing properties of the polymers differ significantly from each other, the laser irradiation strategy may additionally need to be adapted [16,17]. To be able to tailor the material composition and distribution within a powder layer, two different approaches were mainly applied in the past. A two-chamber doctor blade-based powder application device allows the application of two different powder materials simultaneously in the build chamber [17]. However, although this enables the fabrication of multi-material parts using PBF-LB/P, the complexity of these parts is strongly limited due to the simple and non-adaptable border zone between both materials. For this reason, a vibration nozzle-based powder application method was introduced in [18]. Combining several nozzles equipped with different hoppers filled with various powder materials enables the arbitrary deposition of powders into the build chamber [19]. By adjusting the piezoelectric excitation, powder flow properties, surface quality of the sliding surface of the nozzle, cone angle, and orifice diameter, continuous flow and a valve-like start and stop function can be achieved [18,20,21]. However, according to [22], the processing efficiency of nozzle-based powder application processes is relatively low. For this reason, in [23], a hybrid process strategy was demonstrated, joining both the fast powder application possibilities of the doctor blade- or roller-based powder application method for preparing the main powder bed and the selective application of another material by a vibration nozzle. Nevertheless, a major drawback of the nozzle-based powder application remains in the poor homogeneity of the powder layer regarding layer thickness and surface roughness [24]. Processing thermoplastic polymers with different thermal properties requires the generation of complex temperature fields according to the selectively applied materials. As described in [16], three different radiation sources are required for this. While infrared (IR) heaters emitting in the IR spectral range ensure the preheating of low-melting materials, scanner-guided CO<sub>2</sub> laser beams are used for the selective, quasi-simultaneous preheating of polymers with a higher melting temperature. Here, the high deflection speeds of the scanner, on the one hand, and the low thermal conductivity of the plastics, on the other, are used for the homogeneous preheating of the powder bed. A thulium laser in combination with a micromirror array ultimately provides the energy required for the simultaneous melting of both polymer materials [16,17].

### 2.4. Introduction Technology 2: Material-Efficient AM of Multi-Material Polymer Parts through Electrophotography

A promising new approach to overcoming the limitations of conventional or nozzle-based powder application methods is the electrophotographic powder application known from the two-dimensional printing of toner particles in the context of laser printers. Electrophotographic powder application (EPA) for the laser-based powder bed fusion of polymers consists of six main process steps, based on [25–27]. First, the powder and a photoconductive plate (PCP, aluminum plate coated with photoconductive material) are homogeneously charged [28–30]. In EPA, powder particles can be charged via gas discharge or triboelectrically [31–33]. While gas discharge-based powder charging does not require any further functionalization of the particles in terms of their charging behavior, for triboelectric charging, the particles need to be functionalized with charge-control agents (CCAs) [33]. However, as described in [31–33], triboelectric charging offers some considerable advantages compared with gas discharge-based powder charging. In the case

of triboelectric powder charging, the powder flowability, which, in many cases, renders the usage of certain powders impossible for PBF-LB/P, does not play any role in powder application. This allows pharmaceutical polymers or drugs, which often show poor flowability, to be processed in EPA-PBF-LB/P. In the second step of EPA-PBF-LB/P, the PCP is selectively discharged, creating a latent charge pattern by selective illumination.

The current findings are presented in Figure 1. The results show that the achievable surface potential significantly depends on the applied powder-charging strategy. In the case of gas discharge-based powder charging (cf. Figure 1A,B), a threshold behavior is observable, because only a charging voltage of 5 kV (Figure 1B) leads to the creation of a surface potential, which is significantly higher than 0 V. This behavior is attributable to the effect of field ionization, which only appears at sufficiently high electric field strengths and, therefore, charging voltages [26]. In contrast, triboelectric charging (Figure 1C) offers a higher surface potential, which stays constant for a longer time. Both the higher surface potential, as well as the longer duration, are beneficial for EPA-PBF-LB/P and increase the efficiency of this process. In step three of EPA-PBF-LB/P, the so-called development step, charged powder particles are attracted toward the PCP due to electrostatic forces. Depending on the polarity of charging the powder particles in step two, charged particles can either be developed into charged (charged area development, CAD) or discharged (discharged area development, DAD) regions of the latent charge pattern of the PCP. In step four, the printing step, the PCP is moved laterally to the build chamber and the powder pattern is deposited onto the build platform located inside the build chamber. In step five, irradiation by a laser beam takes place to fuse the deposited powder particles. Finally, in step six, the PCP is cleaned. A general demonstration of the working principle of EPA in the context of PBF-LB/P on a single-layer basis was provided in [26,34]. However, printing more than one layer by EPA-PBF-LB/P introduces some challenges, mostly related to the electrostatic phenomena taking place during EPA. As demonstrated in [27], controlling the electric field applied in terms of field strength and especially shape is crucial for powder deposition to achieve high dimensional accuracy and coverage of the deposited powder pattern. Moreover, the accumulation of charges accompanied by a progressive decrease in the electric field strength of the powder deposition field needs to be compensated for [32]. This necessitates a strategy for compensating for charge accumulation independently of the already generated part's thickness. In case of constant environmental conditions, this should lead to a net charge of zero by the neutralization of contrarily charged ions. In fact, after depositing a powder layer with a certain surface potential, a powder layer with contrary charging, but the same magnitude of surface potential, should be deposited on top of the previous layer. This means that the operating modes of EPA-PBF-LB/P should be regularly changed from CAD to DAD. Although changing the polarity after each powder deposition would be even more efficient regarding the compensation for charge accumulation, a certain duration is needed for the reversion of polarity by the high-voltage power supply. In [32], changing the operation mode from CAD to DAD after every second powder deposition was demonstrated to have a good trade-off between duration for the reversion of polarity and still maintaining significant part height growth. A further aspect of increasing the powder deposition efficiency is the development and implementation of a piezoelectric excitation device in [35]. By decreasing the van der Waals interaction forces due to a rapid increase in the separation distance between powder particles using a piezoelectric excitation, the powder deposition efficiency could be significantly enhanced. It is important to note that, in the case of conventional powder application methods, only a small portion of the powder in the build chamber is used to generate the actual part [17]. The remaining powder must be recycled at great expense. As EPA offers the possibility to selectively apply only the powder volume necessary for generating the desired part, EPA-PBF-LB/P can significantly reduce the environmental impact of PBF-LB/P. Beyond that, the number of powder materials applicable for PBF-LB/P can be increased due to the independency of the powder flowability—especially in the case of triboelectric charging. In [32], the parts generated by EPA-PBF-LB/P could be validated to show at least the same

or better mechanical properties compared with parts generated by conventional PBF-LB/P (cf. Figure 2A,B).

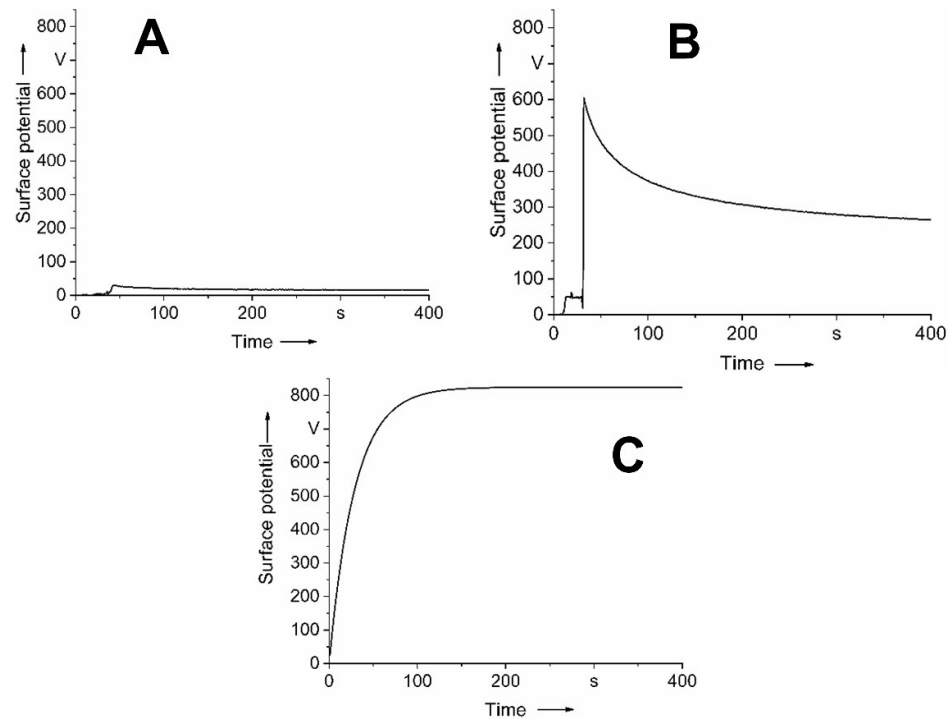


**Figure 1.** Surface potential of a charged polypropylene (PP) powder layer in case of (A) gas discharge-based powder charging with a charging voltage below 4 kV, (B) gas discharge-based powder charging with a charging voltage of 5 kV, and (C) triboelectric powder charging; surface potential measurements were conducted using an electrostatic voltmeter (Monroe 244A, Monroe Electronics Inc., Lyndonville, NY, USA) with a measurement accuracy of 0.1% at a separation distance between the probe and the powder bed surface of 3 mm.

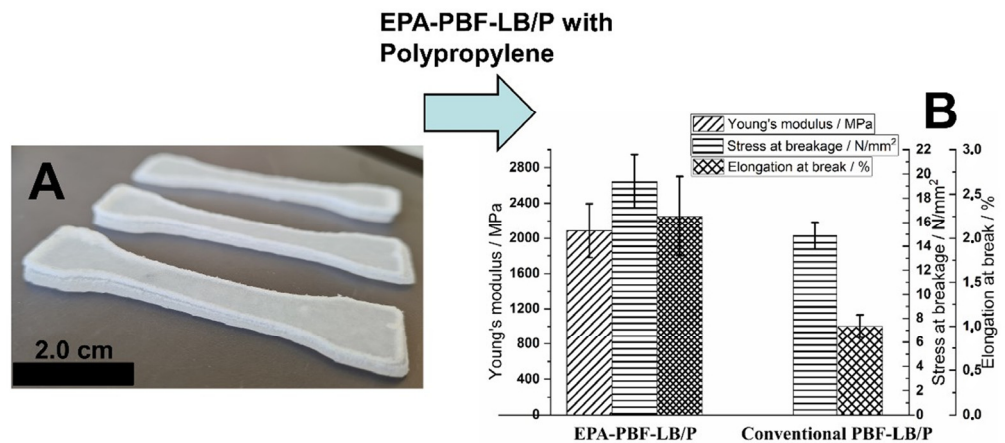


**Figure 2.** (A) Polypropylene (PP) tensile test specimen generated by EPA-PBF-LB/P, (B) mechanical properties of the tensile test specimen shown in (A) (error bars indicate standard deviation of 3 measurements; values for conventional PBF-LB/P from [36]); all images are property of Bayerisches Laserzentrum GmbH and were first published in [32].

The selective and precise powder deposition enabled by EPA further allows the generation of multi-material parts with graded transition zones between the single materials. The part consists of PA12 (PA2200, EOS GmbH, Krailling, Germany) dyed with 0.1 wt% chrome oxide green (Chromoxidgrün, Kremer Pigmente GmbH & Co. KG, Aichstetten,

Germany) and iron oxide red (Eisenoxidrot 110 M, hell, Kremer Pigmente GmbH & Co. KG, Aichstetten, Germany). The processing parameters are given in detail in [32]. It is important to mention that, for the parts shown in Figure 2, EPA allowed only the application of the amount of powder to the build chamber, which actually formed the part. Thus, the filling of the complete build chamber, as is the case with conventional PBF-LB/P, can be avoided by EPA, leading to a nesting efficiency close to 100% [32].

### *2.5. Multi-Material Additive Manufacturing of Thermoset and Thermoset/Thermoplastic Polymer Parts*

The state of the art of multi-material AM with plastics can be divided into two groups: thermoplastics combined with thermoplastics and thermosets combined with thermosets [37]. Examples of thermoplastic-based multi-material AM are mostly represented by material extrusion [38,39] and, as described before, by PBF-LB/P. For thermosets, multi-material AM is mostly represented by technologies like vat photopolymerization [40] and MultiJet modeling [41]. Choi et al. [40] developed a rotating vat system to combine different thermosets in laser-based vat photopolymerization. Bartlett et al. [42] and Boopathy et al. [43] demonstrated the utilization of hard/soft structures by combining different UV-curable thermosets in a broad range of stiffnesses with MultiJet modeling for robotic applications. Also, Moore and Williams [44] et al. investigated the fatigue properties of thermoset multi-material parts created through MultiJet modeling. Besides individually demonstrating numerous potentials in multi-material AM, the combination of thermosets and thermoplastics within a single AM process is not applicable yet. The first attempts have been made to utilize hybrid AM to create thermoset/thermoplastic parts. Dorigato et al. [45] combined thermoplastic structures with an epoxy matrix. The epoxy matrix was implemented and cured within a conventional molding process, which restricted the achievable complexity of the thermoset component. One of the first AM technologies to simultaneously process thermosets and thermoplastics is represented by the so-called “Fusion Jetting” (FJ) process. The FJ technology surpasses previous multi-material AM technologies by achieving outstanding complexities with either material component. The process was first proposed by Wudy et al. [46] and is introduced in the following section.

### *2.6. Introduction Technology 3: Implementation of UV-Curable Thermosets within Laser-Based Powder Bed Fusion of Plastics*

The FJ process combines two powder-based AM processes: laser-based powder bed fusion of plastics (PBF-LB/P) and binder jetting (BJT). Applications lie in the field of hard-soft structures, smart structures, and the introduction of secondary material properties, like thermal and electric conductivity. Also, graded transitions between the materials can be achieved. Figure 3 shows a schematic representation of the steps of the FJ process. The process starts with the initial recoating of a new thermoplastic powder layer, followed by the selective deposition of the liquid photopolymer. After that, the photopolymer is cured with a UV lamp and the surface temperature of the powder bed is subsequently increased with infrared lamps. Once the desired surface temperature is reached, a CO<sub>2</sub> laser is used to selectively melt the thermoplastic powder. The first investigations were conducted to analyze the curing behavior and the thermal stability of acrylate photopolymers with the subsequent modeling of the curing kinetics [47,48]. Subsequent investigations [49] demonstrated that the infiltration behavior of acrylate photopolymers within a thermoplastic polymer powder bed was highly dependent on the surrounding temperature and could be mathematically approximated through an evolved version of the Washburn equation [50]. The bulk density was proven to have a low impact on the infiltration speed. Instead, the choice of material (comparison between PA11 and PEBA), as well as the packing conditions of the powder regarding the manufacturing process of the powder feedstock (grinding vs. chemical precipitation), was proven to have a high impact on the infiltration speed. For the acrylate photopolymers analyzed, no signs of unwanted curing have been detected at temperatures above 100 °C, with respective infiltration times below 500 μs. Also, the dynamic mechanical behavior of photopolymers blended with non-melted thermoplastic

powder was characterized, demonstrating a decrease in the mechanical properties with increasing powder content within the thermoset matrix [51].

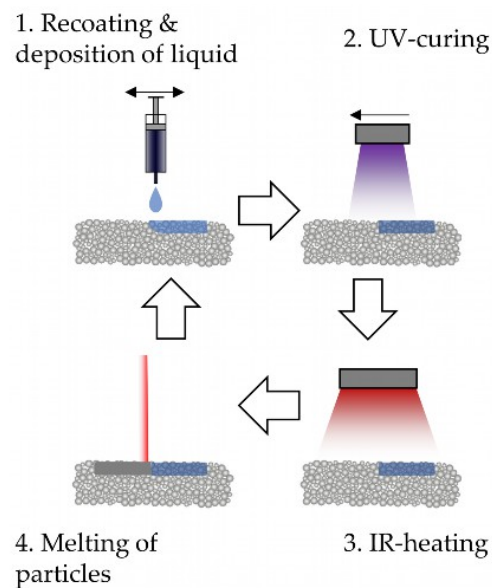


**Figure 3.** Schematic representation of the steps of the FJ process first described by Wudy et al. [46].

Following investigations [52] demonstrated the production of first-generation multi-material parts consisting of thermoplastic polyurethane (TPU) and acrylate-based photopolymers (Figure 4A). Neither the thermoset nor the thermoplastic components of the printed parts showed significant restrictions regarding achievable complexities. Single-layer and multi-layer experiments were performed and microscopically analyzed (Figure 4B).

The results showed that the processing sequence had a high impact on the infiltration behavior and the surface quality of the thermoset-infused layers. BJT layers deposited on PBF-LB/P layers showed restricted infiltration behavior due to the already melted regions, which resulted in higher layer density. The variation in the laser power showed that lower laser powers and, therefore, higher part porosity promoted the infiltration of the liquid photopolymer within previously melted regions. This can be seen as a potential process strategy to decrease delamination behavior in photopolymer-reinforced regions, which was detected during tensile testing (Figure 4C,D). The tensile testing showed that, by increasing the filler content of acrylate photopolymer within the TPU parts, the Young's modulus was increased significantly. Therefore, parts with locally adapted and increased stiffness for small deformations are possible to manufacture with FJ technology. On the contrary, the tensile strength and elongation at break were reduced for photopolymer-reinforced specimens. As mentioned before, the tensile tests demonstrated strong delamination behavior and partial failure within the reinforced regions. This introduces the need for a focused examination of the interconnection between the materials and the transition area. The comparability and transferability of the characterization method toward other technologies and processes should be given. Through this approach, the reduction in the layer connection can be thoroughly characterized. In the following section, an overview and discussion are presented that summarize the state of the art and research on the mechanical testing of multi-material parts.

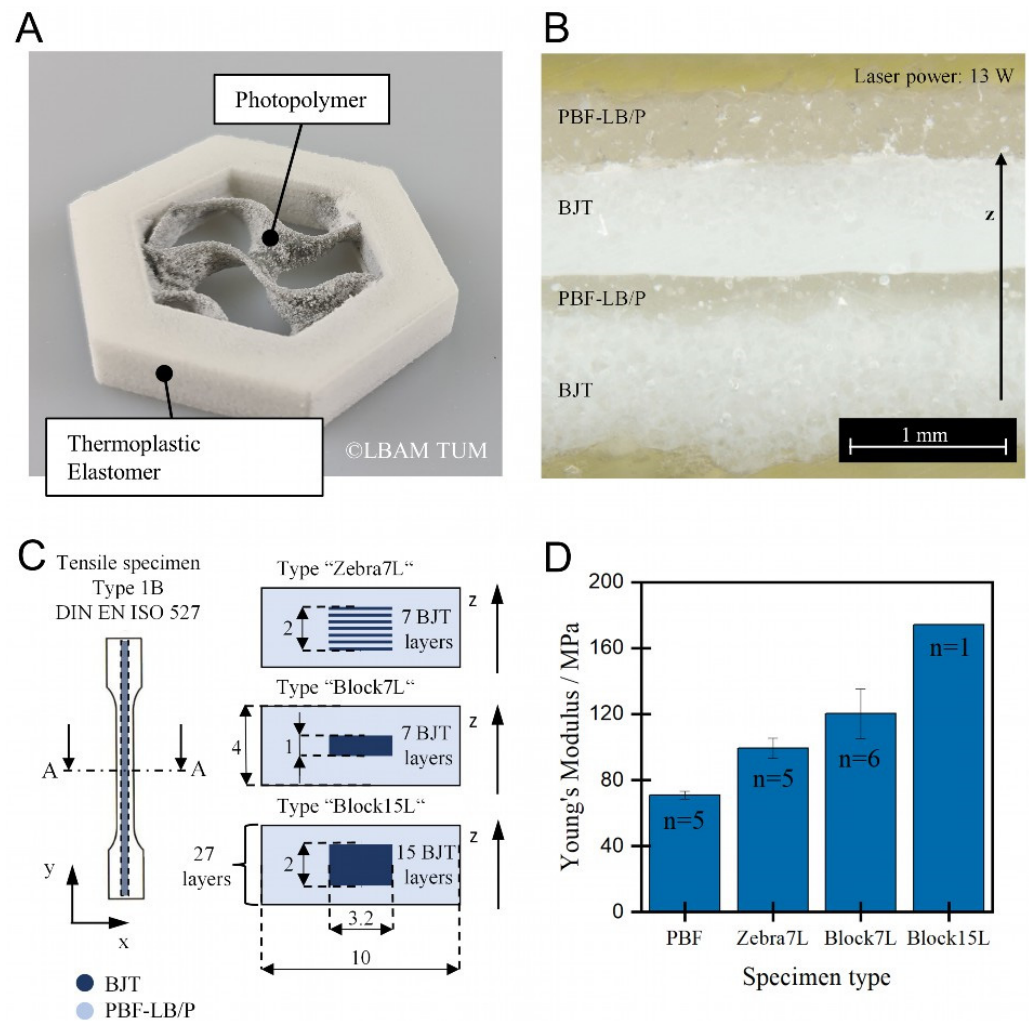


**Figure 4.** (A) Complex multi-material part combining thermoset photopolymers and thermoplastic elastomers, (B) transition areas between thermoset photopolymers and thermoplastic elastomers for a constant laser power. (C,D) different tensile specimen designs and effect of the specimen types on the Young's modulus (all images are property of the Professorship of Laser-based Additive Manufacturing and were first published in [52]).

### 3. Common Challenge of Multi-Material AM: Mechanical Characterization of the Transition Area between Materials

An important takeaway and common challenge of the previously introduced processes are the sufficient characterization of the bonding quality between the additively combined materials. Therefore, extensive research must be invested in the mechanical testing of multi-material parts, with a focus on the transition area between the materials. However, the number of state-of-the-art testing principles for the mechanical testing of multi-material parts is rather low. The possible reasons for this are the novelty of multi-material parts on the one hand, and on the other hand, the composition of multi-material parts. Owing to their nature, multi-material parts consist of two or more materials. The intention of combining different materials lies in their beneficial properties as a compound. This is why multi-material parts are tested as a whole to determine their global properties. However, the results only describe the material's behavior as a whole with the combined properties. A different approach is to identify the single properties of each component. The results are again not descriptive regarding the global properties. Although the combination of principles provides a reasonable way to relate the two individual results, the interaction between both materials is not directly considered. The bonding strength between the materials is critical in terms of the part's overall performance [53]. Therefore, additional testing set-ups

must be used. The number of approaches to investigating the mechanical properties of multi-material parts is limited regarding the analysis of joint strength. Shearing poses a critical state of stress to joints, which is why it is important to test this load case. The used shear test set-up of this investigation is described in the following and is shown in Figure 5.

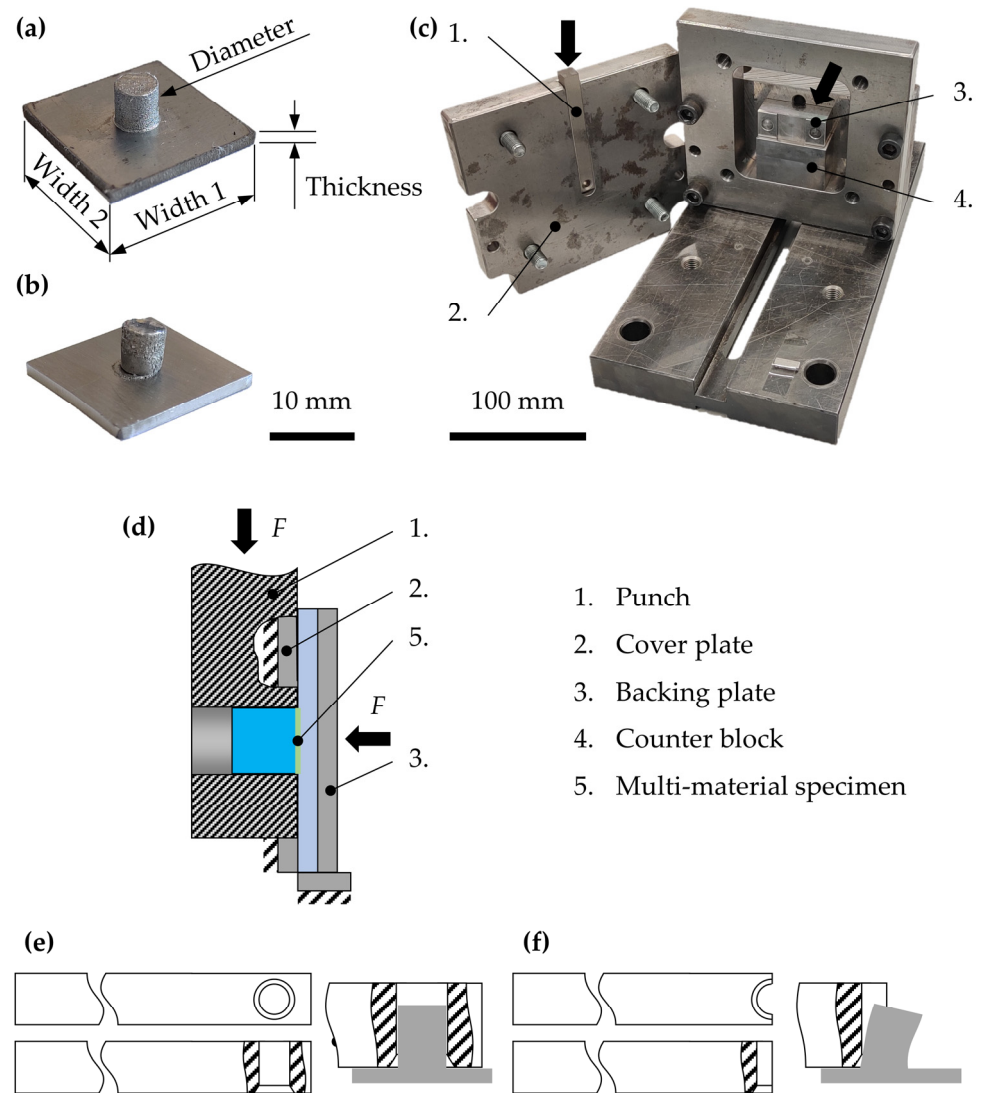


**Figure 5.** (a) Shear test specimen with adaptable dimensions, (b) shear test specimen after the test, (c) tool set-up of the shear tests, (d) schematic illustration of the applied force and used counter-bearings, (e) adapted punch geometry, (f) previous punch geometry.

### 3.1. Experimental Set-Up: Shear Testing of Multi-Material Parts

The experimental setup used in this investigation is depicted in Figure 5. It is an adaption of the set-up presented in [54], where it is used for AM parts composed of a titanium sheet and an additive structure (Figure 5a,b). The specimens were clamped between the cover plate and the backing plate to prevent movements in the axial direction of the cylinder. Clamping forces were set to be low enough to not create friction between the specimen and the punch. With the cylindrical functional elements placed in the hole of the punch, a Z10 universal testing machine from the company ZwickRoell was used to move the punch downward with a constant speed of 1 mm/s, shearing the cylinder of the sheet. This machine offers a maximum force of 10 kN, which is beneficial for polymer parts due to the high resolution at lower force levels. The hardened punch allows for testing materials with higher strength, e.g., steels and other metals. Unlike polymer parts, metal

parts usually require a testing machine with higher maximum forces, which is why the tests with the titanium parts were performed with a model Z100 from the company ZwickRoell with a maximum testing force of 100 kN. The specimens were sheared until a drop in force indicated failure in terms of crack formation and propagation. The applied force and the traveled distance were recorded and could be used to determine the shearing force and stress. In contrast to prior investigations with this set-up [54] (Figure 5f), the punch geometry was adapted to reduce the tilting of the cylinder during testing to a minimum, leading to an almost ideal shearing stress in the joint between the sheet and functional element (Figure 5e). Moreover, the specimens had a “sheet” with a 20 mm × 20 mm surface and cylindrical elements with a diameter of 5 mm and a height of 5 mm. The quadratic shape of the “sheet” was used to prevent deformations in it due to local stresses. Further information regarding the specimen design is described in the next section. The set-up offers a precise analysis of joint strength for hybrid and multi-material parts with a reduced amount of preparation. Moreover, further adaptations to the tools can be easily made due to the modularity of the setup. It is, therefore, possible to test parts with different diameters, sheet thicknesses, and even shapes of the functional elements.

### 3.2. Specimen Design

#### 3.2.1. Metals

Based on the descriptions in Section 3.1, specimen designs for metal multi-material samples were derived, which are depicted in Figure 6, and processed with PBF-LB/M for future use in hybrid AM and vibrational microfeeding (compare with Section 2.2). The specimens consisted of square sheet metal with a side length of 20 mm. The austenitic stainless steel 316L (1.4404), the deep-drawing steel DC04 (1.0338), and the dual-phase steel DP600 (1.0941) were used as the substrate sheets, as shown in Figure 6.

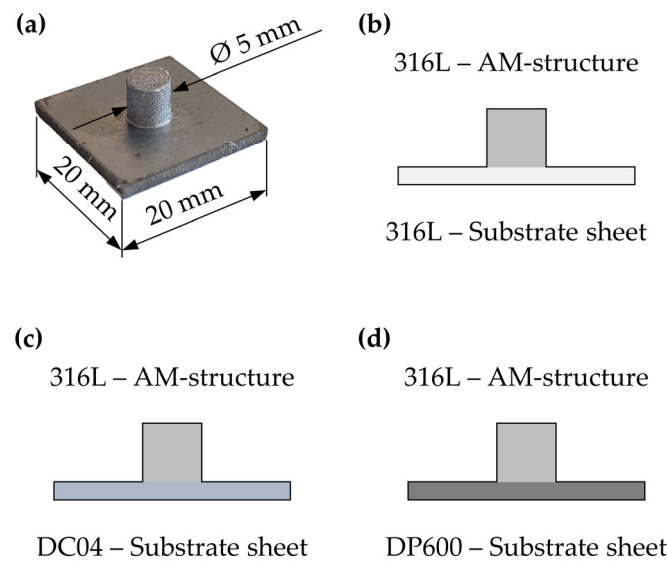


**Figure 6.** (a) Geometric properties of metal-based multi-material AM parts for shear testing, (b–d) material combinations for metal-based multi-material AM parts.

The functional elements had a diameter of 5 mm and a height of 5 mm. Three different sheet metals were used for building the functional elements of 316L powder upon them. The PBF-LB/M process with a volume energy of 127 J/mm<sup>3</sup> was performed on a DMG Mori Lasertec 30 SLM.

#### 3.2.2. Polymers

Based on the descriptions in Section 3.1, specimen designs for polymer multi-material samples were also derived, which are depicted in Figure 7 and were processed by the FJ

technology (compare with Section 2.4). The parts combined acrylate photopolymers (UV DLP Hard, Photocentric 3D, Peterborough, UK) with TPU (TPU 1301, EOS GmbH, Krailling, Germany). The materials are referred to as acrylate photopolymer and TPU throughout this investigation. The individual material values of the respective components can be found in Table 1. Four different sample types were created: reference samples consisting of sole TPU, as well as reinforced samples with different photopolymer geometries in the transition area. The goal was to generate informational output concerning the impact of the different bonding geometries on the interlaminar connection. Before processing, a photopolymer infill of 50% was mathematically generated within the circular cross-section of the sample cylinder with a diameter of 4 mm. For the calculations, a line width of 0.3 mm of the photopolymer was assumed. As can be seen in Figure 7, a spiral pattern, an alternating rectangular pattern with 0°/90° orientation, and a honeycomb pattern were used for cross-sectional photopolymer reinforcement. All lines were created continuously, only resulting in overlaps for the 0°/90° pattern at the intersection points. The material ejection over 30 s was targeted at 250 mg for uniform results. All other processing parameters are summarized in Table 2. The processing sequence followed the process steps presented in Figure 3. Therefore, after the recoating step, every reinforced layer was injected with photopolymer first, followed by complete laser-based material processing of the whole cross-section. All samples of one type were printed at the same time.

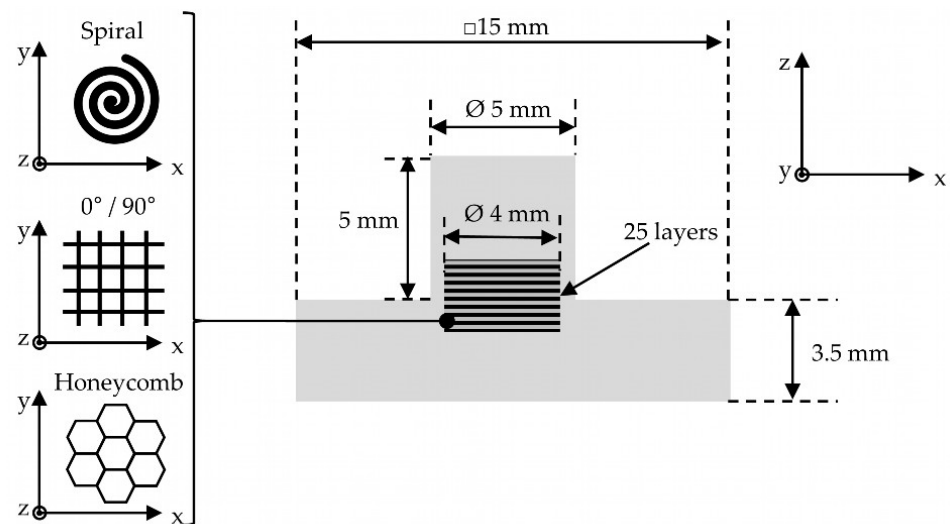


**Figure 7.** Shear specimen design for reinforced multi-material polymer samples combining acrylate photopolymers and thermoplastic polyurethane (TPU), with the variation in the reinforcement geometry within the transition area (spiral, 0°/90°, and honeycomb).

**Table 1.** Significant material values derived from [55,56].

	Acrylate Photopolymer	TPU
Tensile strength/MPa	15	7
Elongation at break/%	4	250
Young's modulus/MPa	2060	60
Melting point/°C	-	138
Viscosity/mPas	230	-
Density/g/cm <sup>3</sup>	1.19	1.11

**Table 2.** Process parameters for test specimen manufacturing divided by general parameters, as well as PBF-LB/P and BJT-related parameters.

General Process Parameters		PBF-LB/P-Related Process Parameters		BJT-Related Parameters	
Layer height/mm	0.1	Scanning speed/mm/s	2500	Resin temperature/°C	55–60
		Laser power/W	15	Print head pressure/bar	2
Process sequence/-	BJT→PBF	Laser hatch distance/μm	250	Nozzle-opening time/μs	190–210
		Laser hatch strategy/-	0°/90°	Nozzle frequency/Hz	200–220
Number of specimens per geometry/-	4	Building chamber temperature/°C	105	Print head speed/m/min	3.8
		Building surface temperature/°C	136	Geometrical layer infill/%	50

#### 4. Experimental Results

##### 4.1. Metals

Regarding the metal-based multi-material AM parts, different sheet metals were investigated for the joint strength between the substrate and functional element. The shearing tests were performed with a constant punch displacement of 5 mm/min on the setup depicted in Figure 5. Before testing, the diameters of the specimens were measured to calculate the resulting joint strength. The average diameters of the functional elements are shown in Figure 8 alongside the force-displacement curves under shearing loads.

As the same powder and PBF-LB/M-parameters were used for the manufacturing of the functional elements, the diameters showed no differences (Figure 8a). The rough surface, which could be attributed to the sintered parts on the surface of PBF-LB/M-parts, led to an increase in size. The real diameter of the parts was 0.4 mm bigger than the designed 5.0 mm. These diameters could be used to calculate the present stresses during testing by dividing the applied force by the area of the cross-section. The forces for each of the material combinations during formation are shown in Figure 8b. The curves showed the same trends, beginning with a rather soft increase, followed by a steeper slope, and a decreased slope until the force decreased at the fracture. The beginning of the curve was characterized by the setting procedure, including the flattening of the mentioned particles at the surface of the parts. The subsequent increase in slope was attributed to the elastic deformation of the functional elements, followed by the plastic deformation (reduced slope). In the end, the force decreased when the plastic deformations were too high and the material tore at the joint. When comparing the different material combinations, certain differences were visible. The parts made with a DP600 substrate sheet material showed the steepest slope during the elastic phase of the shearing test, which was caused by it having the highest strength of the three materials. In addition to that, the slope of the other two materials decreased according to their strength. The lowest strength was found for DC04 and 316L lied between them. However, during the plastic deformation phase of the shear test, the increase in force was highest for 316L, which could be explained by the high strain-hardening potential of the material. The lowest displacements at fracture were found for DP600. The assumed reason for this was its lower ductility compared with the other two materials, which led to a lack of deformation before fracture. Supporting this finding is the fact that the highest displacement was found for DC04, which had the highest ductility of the three materials. In terms of comprehensibility, the maximum forces and resulting stresses are shown in additional diagrams in Figure 9.

The maximum forces (Figure 9a) and stresses (Figure 9b) showed the same trend. The highest forces were found for 316L and the lowest for DP600, which is not proportional to the strengths of the material. Owing to the highest strength of DP600, the joint strength could be expected to be the highest as well. Therefore, the joint strength of the material did not only depend on the strength of the substrate, but rather on more factors. Derived from the force-displacement curves in Figure 8b, the required force to shear the functional element off the substrate sheet increased with the punch displacement due to the strain

hardening of the material. Consequently, the hardening behavior of the material, as well as the achievable strains, occurred because of the punch displacement influencing the joint strength. The high ductility of DC04 led to further deformation and, therefore, hardening than that for DP600, for which the fracture happened at a lower punch displacement. However, 316L offered a comparatively high ductility and strain-hardening behavior, leading to a postponed fracture and distinct hardening until that point. This relationship must be considered when designing metal-based multi-material AM parts. Another approach is to adjust the mechanical properties of the functional elements by using a different material for the whole component or certain regions. The latter can be implemented with the presented vibrational microfeeding approach for metal parts or the binder fusion process for polymers.

Functional elements made of 316L with a volume energy of 127 J/mm<sup>3</sup>;  
 Punch velocity for testing: 5 mm/min

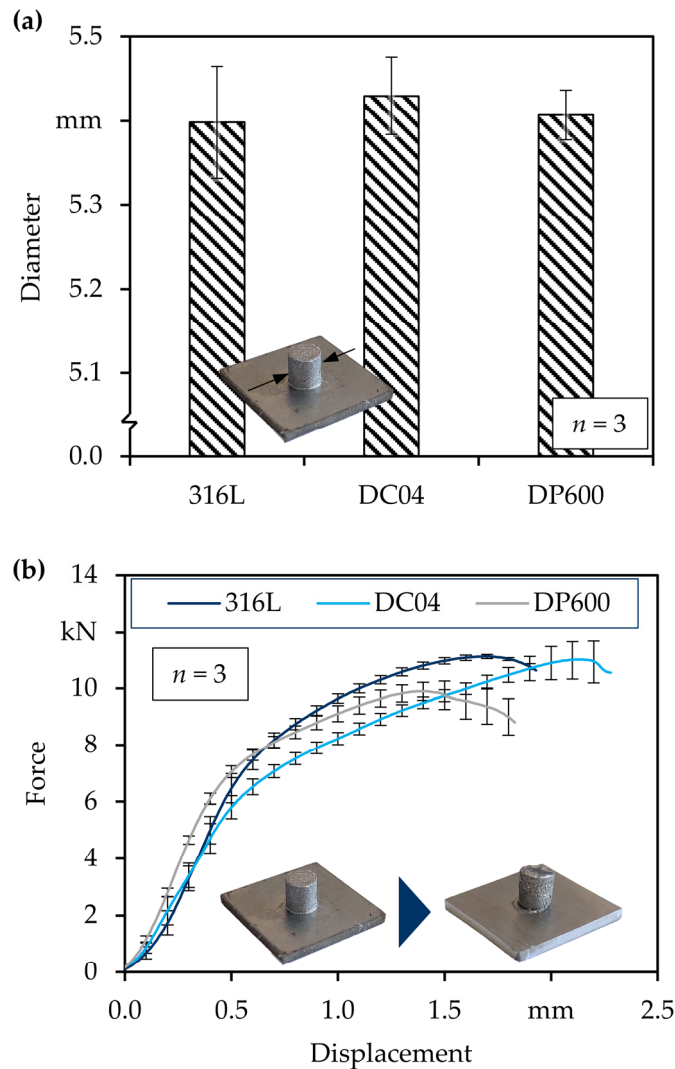


**Figure 8.** (a) Mean diameter of functional elements built on different sheet metal substrates, (b) force-displacement-curves of metal-based multi-material AM parts under shearing load.

Functional elements made of 316L with a volume energy of 127 J/mm<sup>3</sup>;  
Punch velocity for testing: 5 mm/min

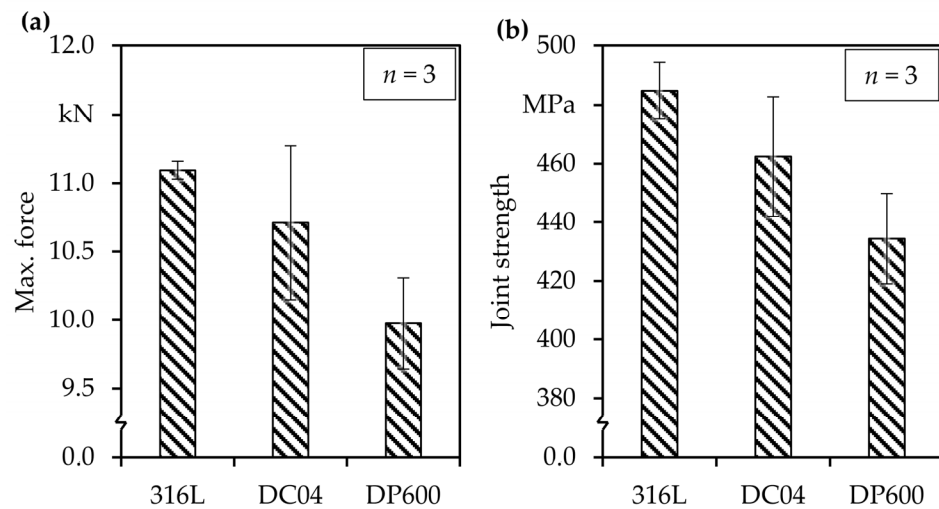


**Figure 9.** (a) Maximum forces during shear testing of metal-based multi-material AM parts, (b) maximum stresses calculated based on the measured diameters and forces.

#### 4.2. Polymers

Figure 10 shows the polymer-based multi-material specimen before and after testing. It can be seen that the part failure was not complete. Instead, the cylinder was only partially detached from the base plate of the specimen. Analysis of the fracture zone indicates that the failure occurred within the photopolymer-reinforced layers of the part.

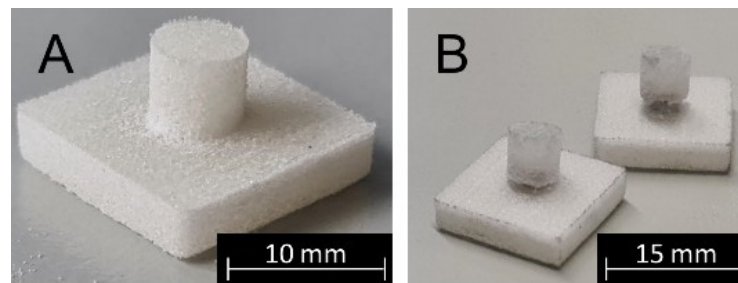


**Figure 10.** (A) Specimen before testing, (B) post-testing specimen with thermoset layers in fracture zone (dark grey; type: spiral).

Before each test run, the diameter of all samples was determined for the determination of the shear strength. The results can be seen in Figure 11. All samples had a slight increase (approximately +0.4 mm) compared with the originally intended geometry of the cylinder diameter. Only mild variations were detectable for all specimen types with the highest deviations for the honeycomb specimen.

Figure 12 shows the average force over the traverse distance. For all specimens analyzed, stable results were achieved regarding the standard deviation. Congruent to the results of [52], the reinforced layers were prone to interlaminar detachment and preliminary failure compared with non-reinforced specimens. The maximum force of the reference samples was more than twice as high compared with that of the reinforced specimens. Also, the achieved traverse distance was nearly twice as high.

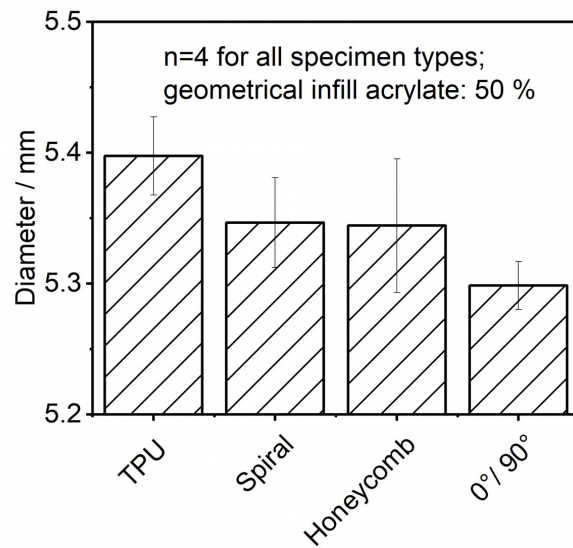


**Figure 11.** Average diameter of the shear specimen of sole TPU samples (reference) and photopolymer-reinforced samples.

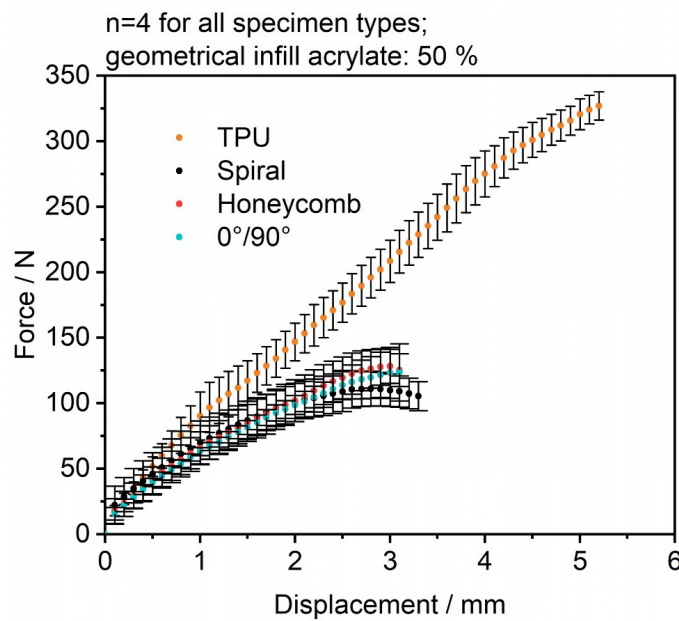


**Figure 12.** Average force over traverse distance of TPU specimen and TPU specimen reinforced with acrylate photopolymer.

To better understand the effect of reinforcement on the specimen shear failure, Figure 13 breaks down the individual progressions of the measured forces over the traverse distance for all photopolymer-reinforced specimens. The honeycomb specimens showed the highest force values compared with the 0°/90° specimen and the spiral specimen, while the spiral specimens had the lowest mechanical values, but achieved the most stable results. The highest fluctuations in material failure were visible for the 0°/90° specimens, which could be potentially correlated to the induced overlaps of the photopolymer lines during processing. Even partial failures were detectable in single cases. In Figure 14, the maximum force values, as well as the resulting maximum shear stress values, are visible. The maximum values and standard deviations are present for the reference samples, while all reinforced specimens showed lower variation regarding their maximum values. The honeycomb reinforcements comparably showed the highest maximum values for the force and stress values of all reinforced specimens. This can be taken as a first step toward future process optimization,

as the results indicate that alternative or combined reinforcement patterns could be utilized to counter interlaminar delamination. In future research, multi-material shear samples created with electrophotographic powder deposition will be analyzed and compared.

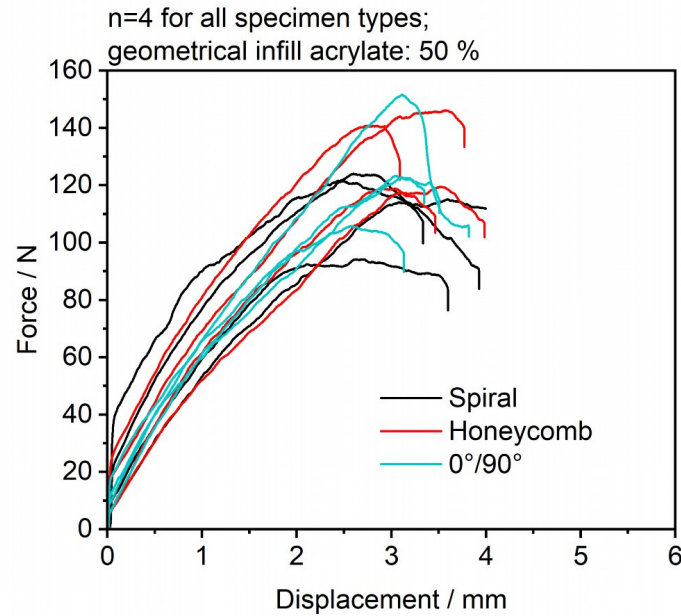


**Figure 13.** Measured force vs. traverse distance for TPU samples reinforced with acrylate photopolymers in different geometric orientations.

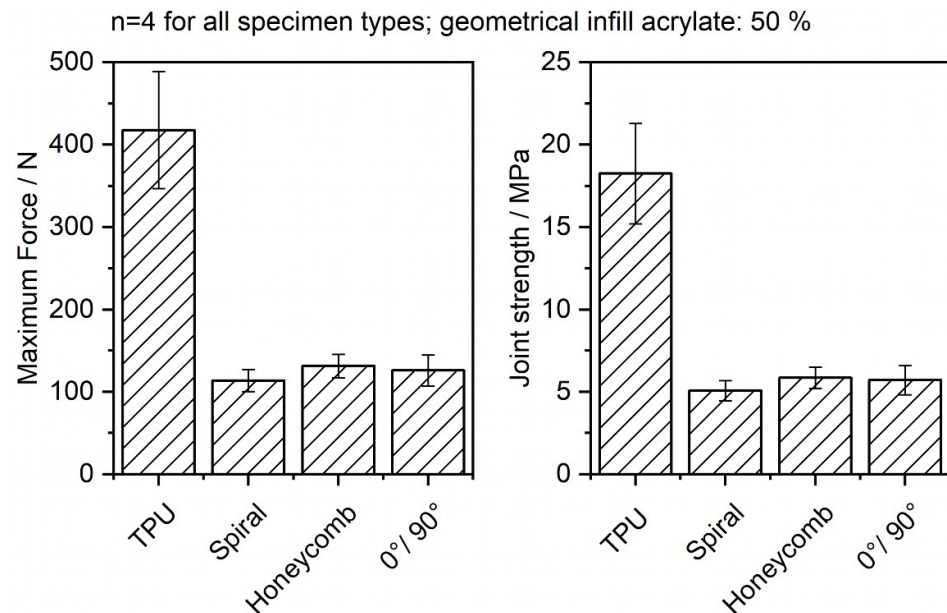


**Figure 14.** Maximum force and stress values detected during shear testing of TPU (reference) and multi-material polymer samples.

### 5. Conclusions

This investigation demonstrated the scientific progress in powder-based multi-material AM based on three successfully utilized experimental technologies in the field of polymer- and metal-based processing. Hybrid AM and vibrational microfeeding in PBF-LB/M, electrophotographic powder application in PBF-LB/P, and the combination of thermoplastics and thermosets with the FJ technology demonstrated the successful creation of multi-material AM parts. Based on the state of technology, the profound analysis of the

transition area between materials was identified as a challenge, as well as a comparable target, for all technologies introduced. However, the number of state-of-the-art testing principles for mechanical testing of multi-material parts along with the transferability of results is limited. Therefore, shear testing with a unified experimental set-up was conducted in the context of this investigation to gather increased information about the quality of the shear strength within the transition area. The shear testing results can be concluded with the following key aspects for the multi-material AM of metals and polymers:

- The combination of 316L and DC04 represents a promising candidate for future hybrid AM, while DP600/316L parts demonstrate reduced bonding behavior compared with conventional 316L/316L parts (metals);
- Confirmation of the assumption that the inclusion of photopolymer reinforcements increases the probability of delamination between reinforced and non-reinforced layers (polymers);
- The geometry of the reinforcing polymer influences the quality of the bonding behavior and represents a promising parameter for future process strategies (polymers).

Furthermore, the selected shear testing set-up represents a sufficient and transferable method for the isolated characterization of the mechanical properties and quality of the transition area. The set-up qualifies for metals and polymers alike, which represents immense potential to comparably characterize multi-material parts and especially the effect of the process parameters on selected regions and graded transitions. This aspect is highly relevant for all technologies discussed in the context of this investigation and future research, as well as other multi-material AM technologies. In the case of hybrid AM with vibrational micro feeding, the results of the investigation will be used as a basis for future combinatory AM processing of 316L with DC04 substrates. Subsequent forming operations and mechanical testing will be performed to qualify and further enhance the performance of the hybrid AM parts. In the field of electrophotographic powder deposition, intensive research will be invested in upscaling the processing speeds in the z-direction, as well as alternative material combinations. In the case of FJ technology, the analysis of the transition area on a microscopic level, as well as the analysis of the (dynamic) mechanical properties, represent important aspects for future investigations. Process parameters, like the energy density, the hatch strategy, the filler content, and the sequence of the individual processing steps, will be strategically varied to demonstrate their significance for the improvement of the mechanical properties and local bonding behavior.

**Author Contributions:** Conceptualization, R.S., J.H., R.R. and S.-P.K.; methodology, R.S., J.H., R.R. and S.-P.K.; validation, R.S. and J.H.; formal analysis, R.S. and J.H.; investigation, R.S. and J.H.; resources, R.S., J.H., M.M. and K.W.; writing—original draft preparation, R.S., J.H., R.R. and S.-P.K.; writing—review and editing, R.S., J.H., R.R., S.-P.K., S.R., M.S., M.M. and K.W.; visualization, R.S., J.H., R.R. and S.-P.K.; supervision, S.R., M.S., M.M. and K.W.; project administration, S.R., M.S., M.M. and K.W.; funding acquisition, S.R., M.S., M.M. and K.W. All authors have read and agreed to the published version of the manuscript.

**Funding:** The authors gratefully acknowledge funding of the Collaborative Research Center 814 (CRC 814) “Additive Manufacturing”, subprojects B5, B6, and B7, as part of working group: “Global and Local Properties” by the German Research Foundation (DFG)—project number 61375930—and of the Erlangen Graduate School in Advanced Optical Technologies (SAOT) by the Bavarian State Ministry for Science and Art.

**Data Availability Statement:** The data presented in this study are available on request from the corresponding author. The data are not publicly available due to privacy restrictions.

**Conflicts of Interest:** The authors declare no conflict of interest.

## References

- Schneck, M.; Horn, M.; Schmitt, M.; Seidel, C.; Schlick, G.; Reinhart, G. Review on additive hybrid- and multi-material-manufacturing of metals by powder bed fusion: State of technology and development potential. *Prog. Addit. Manuf.* **2021**, *6*, 881–894. [[CrossRef](#)]
- Hasanov, S.; Alkunte, S.; Rajeshirke, M.; Gupta, A.; Huseynov, O.; Fidan, I.; Alifui-Segbaya, F.; Rennie, A. Review on Additive Manufacturing of Multi-Material Parts: Progress and Challenges. *J. Manuf. Mater. Process.* **2022**, *6*, 4. [[CrossRef](#)]
- DIN EN ISO/ASTM 52900:2022-03; Additive Fertigung-Grundlagen-Terminologie (ISO/ASTM 52900:2021). Deutsche Fassung EN\_ISO/ASTM 52900:2021. Beuth Verlag GmbH: Berlin, Germany, 2021. [[CrossRef](#)]
- Feenstra, D.R.; Banerjee, R.; Fraser, H.L.; Huang, A.; Molotnikov, A.; Birbilis, N. Critical review of the state of the art in multi-material fabrication via directed energy deposition. *Curr. Opin. Solid State Mater. Sci.* **2021**, *25*, 100924. [[CrossRef](#)]
- Huber, F.; Bartels, D.; Schmidt, M. In-Situ Alloy Formation of a WMoTaNbV Refractory Metal High Entropy Alloy by Laser Powder Bed Fusion (PBF-LB/M). *Materials* **2021**, *14*, 3095. [[CrossRef](#)]
- Anstaett, C.; Seidel, C.; Reinhart, G. Fabrication of 3D multi-material parts using laser-based powder bed fusion. In Proceedings of the 2017 International Solid Freeform Fabrication Symposium, Austin, TX, USA, 7–9 August 2017.
- Wang, D.; Liu, L.; Deng, G.; Deng, C.; Bai, Y.; Yang, Y.; Wu, W.; Chen, J.; Liu, Y.; Wang, Y.; et al. Recent progress on additive manufacturing of multi-material structures with laser powder bed fusion. *Virtual Phys. Prototyp.* **2022**, *17*, 329–365. [[CrossRef](#)]
- Walker, J.; Middendorf, J.R.; Lesko, C.C.C.; Gockel, J. Multi-material laser powder bed fusion additive manufacturing in 3-dimensions. *Manuf. Lett.* **2022**, *31*, 74–77. [[CrossRef](#)]
- Frazier, W.E. Metal Additive Manufacturing: A Review. *J. Mater. Eng. Perform.* **2014**, *23*, 1917–1928. [[CrossRef](#)]
- Hafenecker, J.; Rothfelder, R.; Schmidt, M.; Merklein, M. Stretch Forming of Ti-6Al-4V Hybrid Parts at Elevated Temperatures. *Key Eng. Mater.* **2021**, *883*, 135–142. [[CrossRef](#)]
- Peters, M.; Leyens, C. (Eds.) *Titan und Titanlegierungen*; Wiley-VCH: Weinheim, Germany, 2003; p. 546. [[CrossRef](#)]
- Huber, F.; Papke, T.; Kerkien, M.; Tost, F.; Geyer, G.; Merklein, M.; Schmidt, M. Customized exposure strategies for manufacturing hybrid parts by combining laser beam melting and sheet metal forming. *J. Laser Appl.* **2019**, *31*, 022318. [[CrossRef](#)]
- Huber, F.; Papke, T.; Kauffmann, C.; Rothfelder, R.; Krakhmalev, P.; Merklein, M.; Schmidt, M. Systematic exploration of the L-PBF processing behavior and resulting properties of  $\beta$ -stabilized Ti-alloys prepared by in-situ alloy formation. *Mater. Sci. Eng. A* **2021**, *818*, 141374. [[CrossRef](#)]
- Rothfelder, R.; Lanzl, L.; Selzam, J.; Drummer, D.; Schmidt, M. Vibrational Microfeeding of Polymer and Metal Powders for Locally Graded Properties in Powder-Based Additive Manufacturing. *J. Mater. Eng. Perform.* **2021**, *30*, 8798–8809. [[CrossRef](#)]
- Rothfelder, R.; Huber, F.; Schmidt, M. Influence of beam shape on spatter formation during PBF-LB/M of Ti6Al4V and tungsten powder. *Procedia CIRP* **2022**, *111*, 14–17. [[CrossRef](#)]
- Laumer, T. Realization of Multi-material Polymer Parts by Simultaneous Laser Beam Melting. *J. Laser Micro/Nanoeng.* **2015**, *10*, 140–147. [[CrossRef](#)]
- Laumer, T.; Stichel, T.; Amend, P.; Schmidt, M. Simultaneous laser beam melting of multimaterial polymer parts. *J. Laser Appl.* **2015**, *27*, S29204. [[CrossRef](#)]
- Stichel, T.; Laumer, T.; Baumüller, T.; Amend, P.; Roth, S. Powder Layer Preparation Using Vibration-controlled Capillary Steel Nozzles for Additive Manufacturing. *Phys. Procedia* **2014**, *56*, 157–166. [[CrossRef](#)]
- Wei, C.; Li, L. Recent progress and scientific challenges in multi-material additive manufacturing via laser-based powder bed fusion. *Virtual Phys. Prototyp.* **2021**, *16*, 347–371. [[CrossRef](#)]
- Chen, X.; Seyfang, K.; Steckel, H. Development of a micro dosing system for fine powder using a vibrating capillary. Part 1: The investigation of factors influencing on the dosing performance. *Int. J. Pharm.* **2012**, *433*, 34–41. [[CrossRef](#)]
- Jiang, Y.; Matsusaka, S.; Masuda, H.; Qian, Y. Development of measurement system for powder flowability based on vibrating capillary method. *Powder Technol.* **2009**, *188*, 242–247. [[CrossRef](#)]
- Seidel, C.; Anstaett, C. Next Step in Laser-Based Powder Bed Fusion—Multi Material Processing. *Laser Tech. J.* **2016**, *13*, 21. [[CrossRef](#)]
- Glasschroeder, J.; Prager, E.; Zaeh, M.F. Powder-bed-based 3D-printing of function integrated parts. *Rapid Prototyp. J.* **2015**, *21*, 207–215. [[CrossRef](#)]
- Wei, C.; Gu, H.; Sun, Z.; Cheng, D.; Chueh, Y.-H.; Zhang, X.; Huang, Y.; Li, L. Ultrasonic material dispensing-based selective laser melting for 3D printing of metallic components and the effect of powder compression. *Addit. Manuf.* **2019**, *29*, 100818. [[CrossRef](#)]
- Kumar, A.V.; Dutta, A.; Fay, J.E. Electrophotographic printing of part and binder powders. *Rapid Prototyp. J.* **2004**, *10*, 7–13. [[CrossRef](#)]
- Stichel, T.; Brachmann, C.; Raths, M.; Dechet, M.A.; Schmidt, J.; Peukert, W.; Frick, T.; Roth, S. Electrophotographic Multilayer Powder Pattern Deposition for Additive Manufacturing. *JOM* **2019**, *72*, 1366–1375. [[CrossRef](#)]
- Kopp, S.-P.; Stichel, T.; Roth, S.; Schmidt, M. Investigation of the electrophotographic powder deposition through a transfer grid for efficient additive manufacturing. *Procedia CIRP* **2020**, *94*, 122–127. [[CrossRef](#)]
- Pai, D.M.; Springett, B.E. Physics of electrophotography. *Rev. Mod. Phys.* **1993**, *65*, 163–211. [[CrossRef](#)]
- Shahin, M.M. Mass-Spectrometric Studies of Corona Discharges in Air at Atmospheric Pressures. *J. Chem. Phys.* **1966**, *45*, 2600–2605. [[CrossRef](#)]
- Matsusaka, S.; Masuda, H. Electrostatics of particles. *Adv. Powder Technol.* **2003**, *14*, 143–166. [[CrossRef](#)]

31. Düsenberg, B.; Kopp, S.-P.; Tischer, F.; Schrüfer, S.; Roth, S.; Schmidt, J.; Schmidt, M.; Schubert, D.W.; Peukert, W.; Bück, A. Enhancing Photoelectric Powder Deposition of Polymers by Charge Control Substances. *Polymers* **2022**, *14*, 1332. [[CrossRef](#)]
32. Kopp, S.-P.; Medvedev, V.; Frick, T.; Roth, S. Expanding the capabilities of laser-based powder bed fusion of polymers through the use of electrophotographic powder application. *J. Laser Appl.* **2022**, *34*, 042032. [[CrossRef](#)]
33. Kopp, S.-P.; Düsenberg, B.; Eshun, P.M.; Schmidt, J.; Bück, A.; Roth, S.; Schmidt, M. Enabling triboelectric charging as a powder charging method for electrophotographic powder application in laser-based powder bed fusion of polymers by triboelectric charge control. *Addit. Manuf.* **2023**, *68*, 103531. [[CrossRef](#)]
34. Stichel, T.; Geißler, B.; Jander, J.; Laumer, T.; Frick, T.; Roth, S. Electrophotographic multi-material powder deposition for additive manufacturing. *J. Laser Appl.* **2018**, *30*, 032306. [[CrossRef](#)]
35. Kopp, S.-P.; Medvedev, V.; Roth, S. Targeted vibration excitation for increasing the powder deposition efficiency in electrophotographic powder application for Laser-based Powder Bed Fusion of polymers. *Procedia CIRP* **2022**, *111*, 55–60. [[CrossRef](#)]
36. Tan, L.J.; Zhu, W.; Sagar, K.; Zhou, K. Comparative study on the selective laser sintering of polypropylene homopolymer and copolymer: Processability, crystallization kinetics, crystal phases and mechanical properties. *Addit. Manuf.* **2021**, *37*, 101610. [[CrossRef](#)]
37. García-Collado, A.; Blanco, J.M.; Gupta, M.K.; Dorado-Vicente, R. Advances in polymers based Multi-Material Additive-Manufacturing Techniques: State-of-art review on properties and applications. *Addit. Manuf.* **2022**, *50*, 102577. [[CrossRef](#)]
38. Khondoker, M.; Asad, A.; Sameoto, D. Printing with mechanically interlocked extrudates using a custom bi-extruder for fused deposition modelling. *Rapid Prototyp. J.* **2018**, *24*, 921–934. [[CrossRef](#)]
39. Ali, M.H.; Mir-Nasiri, N.; Ko, W.L. Multi-nozzle extrusion system for 3D printer and its control mechanism. *Int. J. Adv. Manuf. Technol.* **2016**, *86*, 999–1010. [[CrossRef](#)]
40. Choi, J.-W.; Kim, H.-C.; Wicker, R. Multi-material stereolithography. *J. Mater. Process. Technol.* **2011**, *211*, 318–328. [[CrossRef](#)]
41. Sakhaei, A.H.; Kaijima, S.; Lee, T.L.; Tan, Y.Y.; Dunn, M.L. Design and investigation of a multi-material compliant ratchet-like mechanism. *Mech. Mach. Theory* **2018**, *121*, 184–197. [[CrossRef](#)]
42. Bartlett, N.W.; Tolley, M.T.; Overvelde, J.T.B.; Weaver, J.C.; Mosadegh, B.; Bertoldi, K.; Whitesides, G.M.; Wood, R.J. A 3D-printed, functionally graded soft robot powered by combustion. *Science* **2015**, *349*, 161–165. [[CrossRef](#)]
43. Rajendra Boopathy, V.; Sriraman, A. Energy absorbing capability of additive manufactured multi-material honeycomb structure. *Rapid Prototyp. J.* **2019**, *25*, 623–629. [[CrossRef](#)]
44. Moore, J.P.; Williams, C.B. Fatigue properties of parts printed by PolyJet material jetting. *Rapid Prototyp. J.* **2015**, *21*, 675–685. [[CrossRef](#)]
45. Dorigato, A.; Rigotti, D.; Pegoretti, A. Novel Poly(Caprolactone)/Epoxy Blends by Additive Manufacturing. *Materials* **2020**, *13*, 819. [[CrossRef](#)] [[PubMed](#)]
46. Wudy, K.; Drummer, D. Infiltration Behavior of Thermosets for Use in a Combined Selective Laser Sintering Process of Polymers. *JOM* **2019**, *71*, 920–927. [[CrossRef](#)]
47. Setter, R.; Schmölder, S.; Rudolph, N.; Moukhina, E.; Wudy, K. Modeling of the curing kinetics of acrylate photopolymers for additive manufacturing. *Polym. Eng. Sci.* **2023**, *63*, 2149–2168. [[CrossRef](#)]
48. Setter, R.; Schmölder, S.; Rudolph, N.; Moukhina, E.; Wudy, K. Thermal stability and curing behavior of acrylate photopolymers for additive manufacturing. *Polym. Eng. Sci.* **2023**, *63*, 2180–2192. [[CrossRef](#)]
49. Setter, R.; Riedel, F.; Peukert, W.; Schmidt, J.; Wudy, K. Infiltration behavior of liquid thermosets in thermoplastic powders for additive manufacturing of polymer composite parts in a combined powder bed fusion process. *Polym. Compos.* **2021**, *42*, 5265–5279. [[CrossRef](#)]
50. Washburn, E.W. The dynamics of capillary flow. *Phys. Rev.* **1921**, *17*, 273. [[CrossRef](#)]
51. Setter, R.; Stichel, T.; Schuffenhauer, T.; Kopp, S.-P.; Roth, S.; Wudy, K. Additive Manufacturing of Multi-material Polymer Parts Within the Collaborative Research Center 814. In *Enhanced Material, Parts Optimization and Process Intensification*; Reisgen, U., Drummer, D., Marschall, H., Eds.; Springer International Publishing: Cham, Switzerland, 2021; pp. 142–152.
52. Setter, R.; Wudy, K. Simultaneous processing of thermosets and thermoplastics in additive manufacturing of multi-material polymer parts. In *Proceedings of the Annual Technical Conference—ANTEC, Conference Proceedings, Denver, CO, USA, 27–30 March 2023*.
53. Watschke, H.; Waalkes, L.; Schumacher, C.; Vietor, T. Development of Novel Test Specimens for Characterization of Multi-Material Parts Manufactured by Material Extrusion. *Appl. Sci.* **2018**, *8*, 1220. [[CrossRef](#)]
54. Schaub, A.; Juechter, V.; Singer, R.F.; Merklein, M. Characterization of Hybrid Components Consisting of SEBM Additive Structures and Sheet Metal of Alloy Ti-6Al-4V. *Key Eng. Mater.* **2014**, *611–612*, 609–614. [[CrossRef](#)]
55. EOS-GmbH. *TPU 1301 Technical Datasheet*; EOS-GmbH: Krailling, Germany, 2022.
56. Photocentric-Group. *UV DLP Hard Safety Datasheet*; Photocentric-Group: Peterborough, PE, USA, 2022.

**Disclaimer/Publisher's Note:** The statements, opinions and data contained in all publications are solely those of the individual author(s) and contributor(s) and not of MDPI and/or the editor(s). MDPI and/or the editor(s) disclaim responsibility for any injury to people or property resulting from any ideas, methods, instructions or products referred to in the content.